

Nano-Friction, Stick-Slip and Pull-Out Forces in Nanotube-Multiwalls, -Composites and -Bundles

Nicola M. Pugno

*Department of Structural Engineering, Politecnico di Torino,
Corso Duca degli Abruzzi 24, 10129, Italy
nicola.pugno@polito.it*

ABSTRACT

An analysis to understand and quantify the phenomenon of nano-friction and stick-slip observed during sliding of adjacent shells in multiwalled carbon nanotubes is presented. The contact force and shear stress are found to be strongly non-uniform along the contact length, as a consequence of boundary edge effects. In this context, the theoretically predicted *superlubricity state* seems to be unrealistic for finite-sized objects. We demonstrate that such boundary effects dominate sliding at nanoscale for finite-sized object, making it more similar to a fracture phenomenon than to classical friction. The relationship between contact-force and contact-length is found to be asymptotic, explaining the difference in the observations on nanotube sliding reported in the literature. The pull-out force is quantified and found to asymptotically approach a constant value, rather than to be proportional to the contact surface area, as frequently assumed. The analysis is finally applied to predict the strength and toughness of nanotube-based composites and nanotube-bundles.

1. INTRODUCTION

Carbon nanotubes are fascinating low dimensional systems for nano-electronic and nano-mechanical applications. Nanotube devices such as diode, bucky shuttle, or multiple terminal logic circuits have been proposed in nano-electronics /1-3/, as well as nano-pistons, nano-syringes and nano-rotors in nano-mechanics /4-6/. Nano-electromechanical systems (NEMS) have been presented as the new R&D horizon for electromechanical components /7/. Nanotube-based NEMS reported in the literature include nanotweezers, nonvolatile random access memory (RAM) devices, nanorelays, and rotational actuators /8-12/. In contrast, there has been less experimental study on nanotube tribology /13-16/. As recently emphasized, nanofriction remains a not fully understood phenomenon /17/.

Nano-friction and stick-slip behaviours in multi-walled carbon nanotubes have been experimentally

observed, during relative motion of adjacent shells /15/. Such phenomena were described by using a maximum value for the static and dynamic shear stress acting at the contact surface, as suggested by the decrease of the contact force with decreasing contact length. However, this description corresponds implicitly to assuming a maximum tangential contact force proportional to the contact surface length or, equivalently, an approximately constant contact shear stress distribution. On the other hand, further experimental results /16/ suggested a maximum tangential contact force independent from, rather than proportional to, the contact surface length. The observations reported in /15, 16/ differ both qualitatively and quantitatively, showing a discrepancy in the magnitude of the contact shear stress causing sliding of one order of magnitude.

We present a physical interpretation of the phenomenon, explaining the observed differences. Two different theoretical explanations, based on stress and energy, are presented. According to our results the so-called “nano-friction” between shells of multi-walled nanotubes seems to be more connected to elasticity and fracture mechanics thus to adhesion than to a classical friction phenomenon. The contact shear stress distribution is found to be strongly variable along the contact length with strong end peak concentrations. As an example, we quantify such an end effect for one of the experimental cases investigated in /16/. From an energy balance approach (similar to Griffith’s approach for fracture but including the sliding term) a simple formula to predict the pull-out force of a group of shells is presented, which includes a stick-slip coefficient. It is shown that the analysis can explain the discrepancy observed in the experiments. Such a strong influence of the nanotube ends is consistent with the end peak shear stress concentrations, showing that the end(s) of the internal shells govern the sliding process. From atomistic numerical simulations /17/ we quantified reference values for the stick-slip coefficient for both capped and fractured nanotube ends. Theoretical and experimental observations /15, 16/ are then compared.

It is then shown that the approach could be useful in the future design of linear (or rotational) nanotube based nano-actuators. The analysis is also applied to predict the strength and toughness of nanotube-based composites and bundles, showing that, unfortunately, increasing the nanotube embedded length (also indefinitely) is perhaps not sufficient to reach a pull-out stress as large as the ideal nanotube strength. On the other hand, the phenomenon of the pull-out is demonstrated to be important, perhaps exceptionally so, for increasing the toughness of nanocomposites.

2. CONTACT FORCE AND SHEAR STRESS

We refer to the analysis reported in /18/ (and related references). Let us consider a multi-walled nanotube and assume that a sliding process takes place between two adjacent shells at a given radius $R_i < R < R_e$, where R_i and R_e are the internal and external nanotube radii. Assume that the interaction zone is defined by

$-l/2 < z < +l/2$, with length l and surface area $2\pi Rl$: thus R is the radius at which the sliding occurs; z is the axial coordinate with origin at the middle of the interaction zone, thus migrating during sliding. Note that here l represents the geometric contact length *plus* the additional distance along which there is a non-vanishing van der Waals interaction between the nested shells. To study nano-friction we assume fixed internal shells (with radii smaller than R) and apply a tensile axial force F to the external shells (with radii larger than R) to produce a relative “pull-out”, see Figure 1.

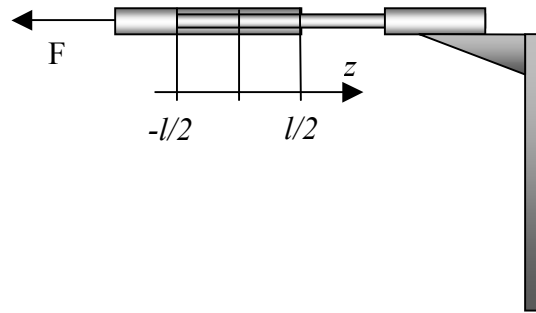


Fig. 1: Pull-out of nanotube external shell: schematic view for the model and reference system.

Under these conditions, the axial equilibrium gives a relationship between the contact shear stress $\tau(z)$ and the variation along the contact length of the axial force $F(z)$ transmitted by a given section z of the external shells, as: $\tau(z) = -\frac{1}{2\pi R} \frac{dF(z)}{dz}$ (equilibrium equation). Note that $F(z = -l/2) = F$, $F(z = +l/2) = 0$, and for the internal shells the force transmitted in the section z is $F - F(z)$. Since the system is analysed as at equilibrium, the potential energy related to the van der Waals contact interactions can be expanded around the equilibrium position up to the second order; this corresponds to assuming a linear relationship between the shear stress τ and strain γ , i.e., $\tau = k^{(vdW)} \gamma$ (constitutive equation), where $k^{(vdW)}$ describes the van der Waals interaction. This is assumed to describe the stress-strain relationship in the interaction zone between inner and outer shells. We assume the “thickness” t of the contact, in analogy to a virtual adhesive, to be infinitesimal. In addition, the longitudinal relative displacement w between internal and external shells at the contact must be compatible with the shear strain in the contact zone, that is:

$$\Delta w(z) = \frac{1}{\pi E} \left\{ \int \frac{F - F(z)}{R^2 - R_i^2} dz + \int \frac{F(z)}{R_e^2 - R^2} dz \right\} + \text{const} = t\gamma(z) \quad (\text{compatibility equation}),$$

where E is the

Young’s modulus of the nanotube shells, see /18, 19/. By derivation of the compatibility equation, coupling it with the constitutive and equilibrium equations, we find the differential equation governing the longitudinal

transmission of the nano-friction force $F(z)$:

$$\frac{d^2 F(z)}{dz^2} - \alpha^2 F(z) + \beta = 0 \quad , \quad \alpha^2 = \frac{2\pi k^{(vdW)} (R_e^{*2} - R_i^{*2})}{tER(R_e^{*2} - 1)(1 - R_i^{*2})} \quad , \quad \beta = \frac{2k^{(vdW)}F}{ER(1 - R_i^{*2})} \quad (1)$$

in which we have introduced the dimensionless radii $R_e^* = R_e/R$ and $R_i^* = R_i/R$. Solving eq. (1) with the related boundary conditions ($F(z = -l/2) = F$, $F(z = +l/2) = 0$), gives:

$$F(z) = F(C_1 e^{\alpha z} + C_2 e^{-\alpha z} + \lambda) \quad ,$$

$$\lambda = \frac{(R_e^{*2} - 1)}{(R_e^{*2} - R_i^{*2})} \quad , \quad C_1 = \frac{(1 - \lambda)e^{-\alpha l/2} + \lambda e^{\alpha l/2}}{e^{-\alpha l} - e^{\alpha l}} \quad , \quad C_2 = C_1 (\alpha \rightarrow -\alpha) \quad (2)$$

Since the friction force is quantified, we can try to make a prediction on its critical value that corresponds to the starting of the pull-out or sliding. First, we assume the contact as quantized, that is, the sliding advances by finite amounts a , a characteristic length for the sliding process. We further assume a quantized version shear stress $\tau_Q / 20l$ rather than a continuous shear stress τ .

$$\tau_Q(z) = \frac{1}{a} \int_z^{z+a} \tau(z) dz = \frac{F(z) - F(z+a)}{2\pi Ra} \quad (3)$$

that must reach a maximum value $\tau_{\max}^{(vdW)}$, characteristic of the van der Waals interaction. From the condition $\tau_{Q\max} = \tau_{\max}^{(vdW)}$ the force that initiates sliding, F_{\max} , can be derived if a value for a is specified. On the other hand, in the limit case of $\alpha a \rightarrow 0$, we obtain the “continuum” approach as $\tau_{\max} = \tau_{\max}^{(vdW)}$. According to our analysis the maximum shear stresses τ are reached at the ends of the contact and the higher stress peak appears at the end of the group of shells (inner or outer) with larger cross-section area. The shear stress is typically assumed to be nearly constant, and thus evaluated as the force divided by the contact surface; according to our analysis this is incorrect. There is a strong difference between mean and maximum quantized shear stress; the maximum value is $\tau_{Q\max} = \tau_Q(z = l^*/2)$ where $l^* = -l$ for $0 < \lambda < \frac{1}{2}$, or $l^* = +l$ for $\frac{1}{2} \leq \lambda < 1$ (i.e., it is reached at the end of the stiffer group of shells), whereas the mean value is

$$\langle \tau_Q \rangle = \langle \tau \rangle = \frac{1}{l} \int_{-l/2}^{+l/2} \tau(z) dz = \frac{F}{2\pi Rl} \quad .$$

Very importantly, for $\alpha l \rightarrow \infty$ the maximum quantized shear stress tends asymptotically to a value

different from zero, i.e., $\tau_{Q_{\max}}^{(asy)} = \lim_{\alpha l \rightarrow \infty} \tau_{Q_{\max}} = \frac{F\lambda(e^{\alpha a} - 1)}{2\pi Ra}$. For a continuum $\tau_{\max}^{(asy)} = \lim_{\alpha a \rightarrow 0} \tau_{Q_{\max}}^{(asy)} = \frac{F\lambda\alpha}{2\pi R}$.

This means that in this asymptotic region (large contact lengths), the nano-friction maximum force is finite and equal to $F_{\max}^{(asy)} = \frac{2\pi Ra\tau_{\max}^{(vdW)}}{\lambda(e^{\alpha a} - 1)}$, and thus it should be observed as independent of contact length and not

proportional to it, as would be found if an essentially uniform stress distribution is assumed. As a consequence, making very long nanotubes will not increase indefinitely the corresponding pull-out forces.

We can also rigorously define the asymptotic region: in particular, assuming $\alpha a \rightarrow 0$:

$$\mathcal{g} = \frac{F_{\max}}{F_{\max}^{(asy)}} = \frac{1/2 + |\lambda - 1/2|}{C_2 e^{-\alpha l^*/2} - C_1 e^{\alpha l^*/2}} \quad (4)$$

from which we estimate the asymptotic region, e.g., $\mathcal{g} > 0.99$, starting from values of αl larger than ~ 6 .

3. ENERGY BALANCE DURING STICK-SLIP SLIDING

According to the contact quantization previously introduced, the energy balance has to be written not considering the differentials (as usually done) but rather considering the finite differences $/20/$. During sliding by a finite quantity a , the finite variation of the sum between the free-energy W of the system, the kinetic energy T and the energy Ω spent to create the new free surface must be zero, thus:

$$\Delta(W + T + \Omega) = 0. \quad (5)$$

From this equation an additional prediction for F_{\max} can be derived. The finite variation of the free-energy of the system during stick-slip sliding must be:

$$\Delta W = \Delta L - F(\Delta w + \eta a) = \Delta \left(\frac{1}{2} Fw \right) - F\Delta w - \eta Fa = -\Delta L - \eta Fa, \quad (6)$$

where ΔL denotes the variation in the elastic strain energy of the nanotube (evaluated by virtue of Clapeyron's theorem); Δw represents the elastic displacement of external force, whereas a is its rigid component, that is the sliding motion. For pure sticking $\eta = 0$, whereas for pure sliding $\eta = 1$: thus in general during stick-slip we expect $0 \leq \eta \leq 1$. We define this parameter as a stick-slip coefficient. We note that the case of $\eta = 0$ corresponds to a fully fracture-mechanics-based interpretation $/18/$, according to the

Griffith's energy balance. Evidently:

$$\Delta\Omega = 2\pi RaG_C^{(vdW)} = ca, \quad (7)$$

where $G_C^{(vdW)}$ is (twice) the energy spent to create the unit surface area under van der Waals interactions (and $c = 2\pi RG_C^{(vdW)}$). We assume quasi-static conditions, i.e., $\Delta T \approx 0$, since we are interested in the incipient sliding force.

According to the previous tensional analysis the sliding will start at the zone where the quantized shear stresses are higher, thus at the end of the group (inner or outer) shells with larger global cross-section area. When a quantized sliding a occurs, the inner and outer shells present an additional length a in tension under F and the contact length is reduced from l to $l-a$; accordingly the elastic strain energy can be written as /18/:

$$L(a) = \frac{1}{2\pi ER^2} \left\{ \int_{-l/2+a/2}^{l/2-a/2} \left(\frac{(F-F(z))^2}{(1-R_i^{*2})} + \frac{F^2(z)}{(R_e^{*2}-1)} \right) dz + \frac{F^2 a}{(1-R_i^{*2})} + \frac{F^2 a}{(R_e^{*2}-1)} \right\}, \quad (8)$$

that are integrals of known functions. Thus,

$$\Delta L = L(a) - L(a \rightarrow 0) = \frac{F^2}{2K} a, \quad (9)$$

where $K = k\mathcal{G}$ is a known constant. Thus, eq. (5) can be rewritten as $\frac{F^2}{2K} + \eta F - c = 0$, from which:

$$\begin{aligned} F_{\max} &= \mathcal{G}F_{\max}^{(asy)}, \\ F_{\max}^{(asy)} &= -\eta k + \sqrt{\eta^2 k^2 + 2ck}, \quad 0 \leq \eta \leq 1, \\ k &= \frac{\pi}{\xi} R^2 E, \quad \xi = \frac{1}{(R_e^{*2}-1)} + \frac{1}{(1-R_i^{*2})} - \frac{1}{(R_e^{*2}-R_i^{*2})}, \quad c = 2\pi RG_C^{(vdW)}. \end{aligned} \quad (10)$$

The parameter \mathcal{G} describing the transition towards the asymptotic region is defined by the integrals in eq. (8); however, it can also be estimated by eq. (4). The force becomes rapidly and basically independent from the contact length; thus, the motion is metastable: the quantum and continuum approaches become here coincident, as shown by the independence of $F_{\max}^{(asy)}$ from a ; consequently, it could be confused with a classical friction phenomenon, occurring at the nanoscale. However, a friction coefficient cannot be

defined, since the (tangential) contact force is observed also under zero normal force and especially such a force is independent of the contact length. Note that if $K \rightarrow \infty$ (nanotube infinitely rigid) and pure sliding is considered ($\eta = 1$) $F = c$, that represents the *surface tension force* of the van der Waals interactions /15/. Moreover, for full sticking $\eta = 0$, the force is similar to the prediction reported in /18/: only a slight difference in the parameter ξ is observed, a consequence of the reversibility of the van der Waals sliding, that in classical fracture does not exist.

4. COMPARISON BETWEEN TENSIONAL AND ENERGY APPROACHES

Let us assume an harmonic sliding interaction of periodicity a in the form of:

$$\tau \approx \frac{k^{(vdW)} a}{2\pi t} \sin \frac{2\pi t}{a} \gamma. \quad (11)$$

so that, for small relative displacements $\Delta w = \gamma t$, we obtain the previously introduced relationship of $\tau = k^{(vdW)} \gamma$. From this equation, it follows that $\tau_{\max}^{(vdW)} \approx \frac{k^{(vdW)} a}{2\pi t}$, and $G_C^{(vdW)} \approx C \tau_{\max}^{(vdW)} a$, where C must be a dimensionless constant. To compare the two approaches (Sections 2,3) let us assume $al \rightarrow \infty; \alpha a, \eta \rightarrow 0$. Introducing the previous relationships in the stress-based approach (Section 2) we obtain the same prediction for $F_{\max}^{(asy)}$ as given by the energy based approach (Section 3), as well as the expression of the constant C . For example, for $R_e^* \approx 1$ and $R_i^* \approx 0$ (e.g., pull-out of the external shell of a large multi-walled nanotube) $C \approx 1$. Thus, even if the two approaches are different and some simplifying assumptions have been made, their results are consistent. On the other hand, in general, in the stress-based approach the values of a and t remain unspecified. Thus, we prefer to focus on the energy-based approach, in which we are more confident, assuming $G_C^{(vdW)}$ identical to the cohesive energy for graphite (thus twice the surface energy), thus: $G_C^{(vdW)} \approx 0.22 \text{ Nm}^{-1}$ /21/ and using η as a numerically (or experimentally) computed parameter. We prefer this rather than using $\eta = 0$ or $\eta = 1$ and $G_C^{(vdW)}$ as a best fit parameter, since the parameter η in our approach has well defined limits and physical meaning.

Future experiments on nanotubes may reveal the existence of *superlubricity state* /22/ in the sliding between neighboring shells. Such a phenomenon is expected when two atomically flat incommensurate surfaces slide relative to each other under zero sliding force. However, our analysis suggests that such a state should be more likely for an infinite sized structure than a finite one, as a consequence of the dissipations of the edges. In addition, rolling rather than sliding, implying a negligible surface generation, would be closer to such a non-dissipative state, as experimentally observed /13, 14/.

5. EXPERIMENTAL COMPARISON

We refer to the atomistic numerical simulations /17/ on sliding in multi-walled nanotubes with both capped and fractured ends, Figure 2. From such simulations we obtain estimations for the stick-slip coefficient: their results are well fitted (fixing $G_C^{(vdW)} \approx 0.22 \text{ Nm}^{-1}$) with $\eta \approx 0.1$ for fractured ends, and with $\eta \approx 0.8$ for capped ends. Since the values are in the range (0,1), our analysis seems to be consistent. Note that the authors did not simulate nanotubes of the same size as the (larger) experimentally investigated nanotubes. The differences observed in the atomistic simulations on pull-out forces for capped and fractured nanotubes suggested the presence of end effects (in contrast to a classical frictional phenomenon), as emphasized by our analysis. In addition, numerical simulations performed considering an external pressure, revealed basically a negligible influence on the pull-out force for nanotubes with capped ends, whereas for fractured ends only a small linear increase of the pull-out force was observed /17/.

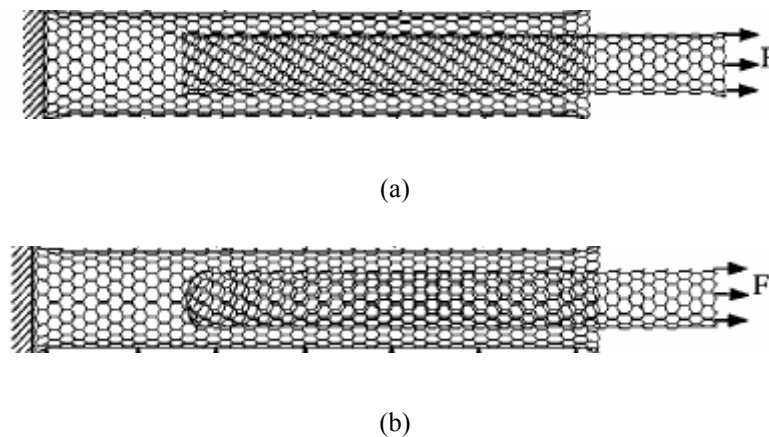


Fig. 2: Pull-out of nanotube external shell with fractured and capped ends as investigated by atomistic simulations in /16/.

We now consider the experimental investigations reported in /15/, in which the sliding, after (sword-in-sheath) fracture of the outer shell /23/, was investigated by gripping multi-walled carbon nanotubes by opposing atomic force microscope (cantilever) tips. We consider also the experimental results presented in /16/, for “not fractured” (and capped) nested nanotubes. The effective contact length l is equal to the geometric contact length l_0 plus the gap length g corresponding to a finite van der Waals interaction, i.e., $l = l_0 + g$. The pull-out of the external shell of a carbon nanotube of diameter equal to 36nm has been

measured by varying the contact length l_0 in the range $0-7.5 \mu\text{m}$. The observed maximum force $F_{\text{max}} \approx 219 \text{ nN}$ was assumed in /17/ to be related to fracture ends. Considering $\eta \approx 0.1$, $E \approx 1 \text{ TPa}$, $G_C^{(vdW)} \approx 0.22 \text{ Nm}^{-1}$, $R_e \approx 18 \text{ nm}$, $R_i \approx 0$, $R \approx R_e - s/2$, where $s \approx 0.34 \text{ nm}$ is the spacing between neighbouring shells, and $l \approx l_0$ we find $F_{\text{max}}^{(asy)} \approx 232 \text{ nN}$. The comparison between theory and experiments is shown in Figure 3 (for experimental details see /15/), from which we deduce $\alpha \approx 3.5 \cdot 10^5 \text{ m}^{-1}$ and thus $l^{(asy)} \approx 6/\alpha \approx 14 \mu\text{m}$ as the extension of the non-asymptotic region. Similar results were obtained by the same authors for a nanotube of diameter equal to 30 nm by varying the contact length in the range $0-2.2 \mu\text{m}$. Considering the previous parameters but $R_e \approx 15 \text{ nm}$, we find $F_{\text{max}}^{(asy)} \approx 193 \text{ nN}$. This asymptotic value was not experimentally measured as a consequence of the short investigated contact length. The comparison with the experimental results is reported in Figure 4, from which we estimate $\alpha \approx 7 \cdot 10^5 \text{ m}^{-1}$, thus $l^{(asy)} \approx 9 \mu\text{m}$. From Figures 3 and 4 the “residual” van der Waals force for negligible geometric contact length l_0 are estimated for the investigated nanotubes to be ~ 20 and $\sim 70 \text{ nN}$, vanishing at separation distances g of ~ 0.5 and ~ 1 microns, respectively. Assuming such “van der Waals” contact lengths of physically separated but still aligned nanotube segments as negligible, implies that the comparisons with experiment become significant for values of l not too small (Figures 3 and 4).

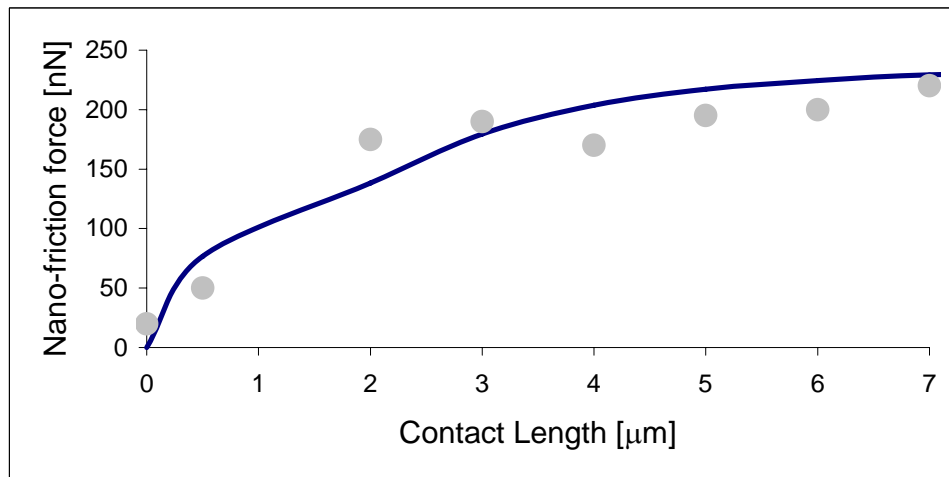


Fig. 3: Nano-friction force F_{max} (causing the sliding) vs. contact length l , as theoretically estimated (line) and experimentally measured (dots), for the 36 nm diameter nanotube with fractured ends.

An experimental analysis is reported in /16/ for a capped end nanotube $\sim 5 \text{ nm}$ in diameter, for contact lengths in the range $0-700 \text{ nm}$. The constant measured force was $\sim 4.1 \text{ nN}$. Considering the same previous parameters but $\eta \approx 0.8$ and $R_e \approx 2.5 \text{ nm}$ we find $F_{\text{max}}^{(asy)} \approx 4 \text{ nN}$. Note that if fractured ends are assumed ($\eta \approx 0.1$) a value larger by approximately one order of magnitude is found, i.e., $F_{\text{max}}^{(asy)} \approx 30 \text{ nN}$. The

comparison is reported in Figure 5. The force remains basically constant until a vanishing contact length is reached and then it goes to zero in $\sim 200\text{nm}$. Thus, we assume $l^{(asy)} \approx 200\text{nm}$ and $\alpha \approx 2.5 \cdot 10^7 \text{ m}^{-1}$. Note the strong difference in the forces with respect to the fractured nanotubes. For the fractured nanotubes the sliding is reduced (lower value of η), and this could be due not only to the difference in the ends (fractured and capped) as postulated in /16/ but more likely to the damage of the external shell after fracture, e.g., as due to “plastic” ribbon formations /24/. The nanotubes in fact were broken only on their external shells and thus there is not any reason to expect fractured ends for the internal shells. This implies that the larger sticking described by the lower value of η could be more likely due to the anchorage of the damaged external shell “zones” on the inner shell.

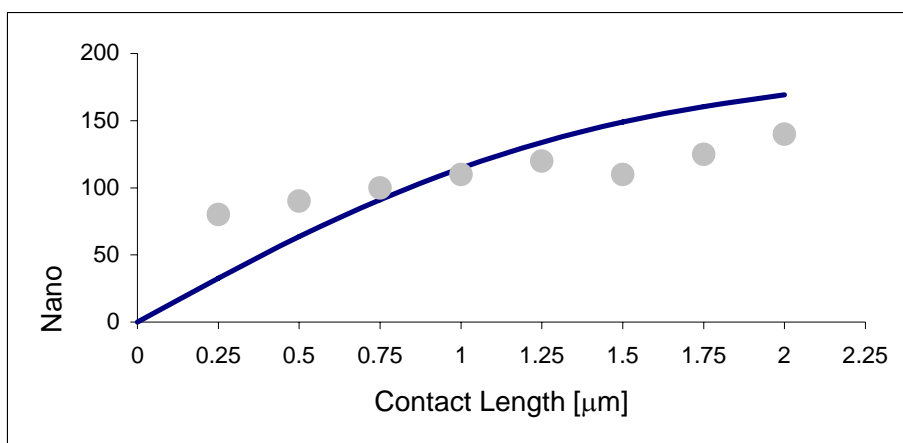


Fig. 4: Nano-friction force F_{max} (causing the sliding) vs. contact length l , as theoretically estimated (line) and experimentally measured (dots), for the 30nm diameter nanotube with fractured ends.

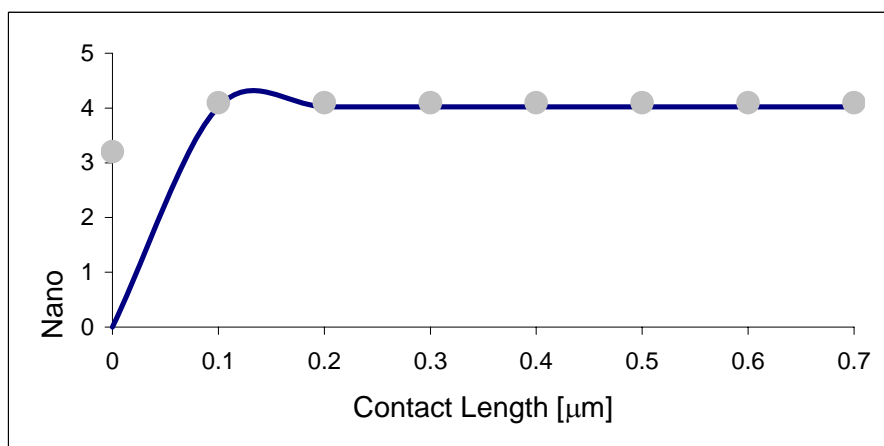


Fig. 5: Nano-friction force F_{max} (causing the sliding) vs. contact length l , as theoretically estimated (line) and experimentally measured (dots), for the 5nm diameter nanotube with capped ends.

To have an idea of the transmission for the nano-friction force and of the shear stress along the contact, let us focus as an example on the first discussed nanotube ($R_e \approx 18 \text{ nm}$), considering the initial case of $l \approx l_0 = 7.5 \text{ }\mu\text{m}$ and assuming a force of $F \approx 232 \text{ Nn}$. The theoretical predictions of the corresponding nano-friction force transmission and of the contact shear stress are reported in Figures 6 and 7. Note that the contact stress presents an end concentration ~ 2.6 times larger than its mean value, which is close to 0.28 MPa : thus the assumption of a constant shear stress along the contact is unjustified. By this assumption we would derive a van der Waals shear strength of 0.28 MPa , whereas probably it could be ~ 3 times larger. Increasing the contact length, the force required to sliding the shell will remain constant, and while the mean shear stress will tend to zero its maximum value will approach the non zero value of $\tau_{\max}^{(asy)} = \frac{F\lambda\alpha}{2\pi R} \approx 14 \text{ KPa}$.

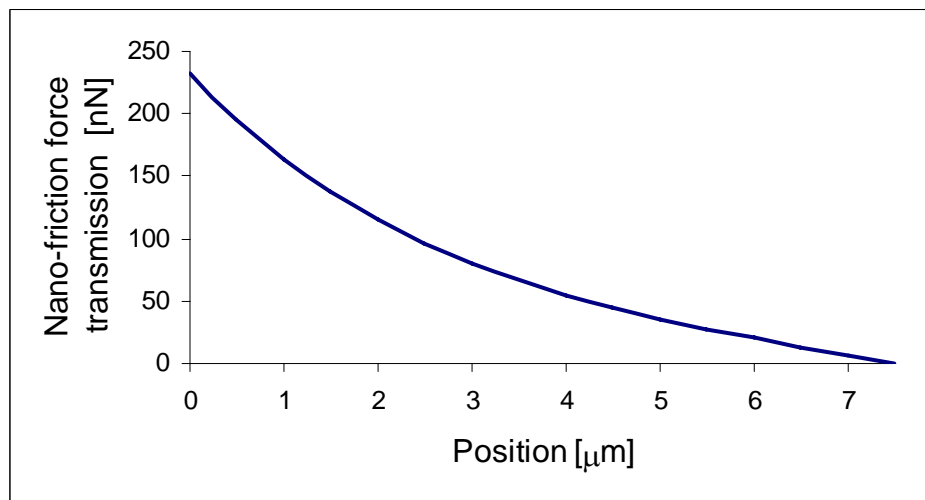


Fig. 6: Nano-friction force transmission $F(z)$ vs. position $z+l/2$, as theoretically estimated for the 36 nm diameter nanotube with contact length $l = 7.5 \text{ }\mu\text{m}$.

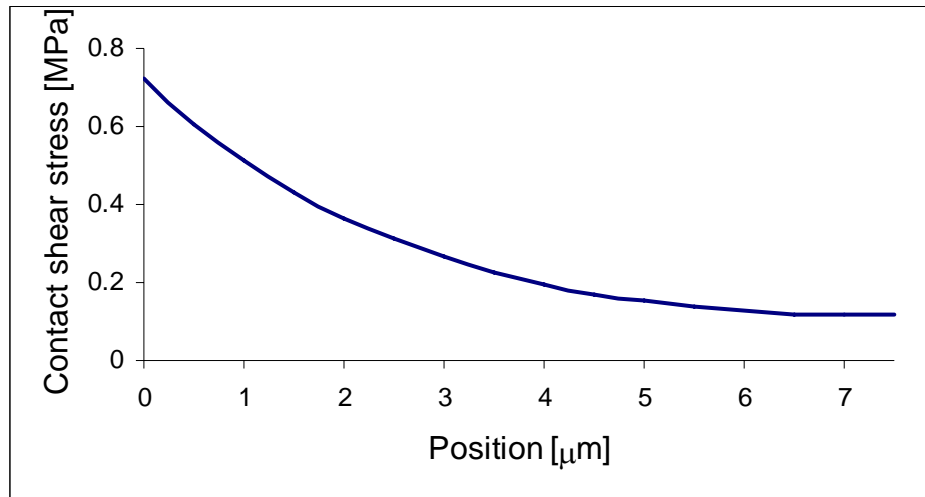


Fig. 7: Contact shear stress $\tau(z)$ vs. position $z+l/2$, as theoretically estimated for the 36nm diameter nanotube with contact length $l = 7.5\mu\text{m}$.

6. APPLICATIONS

Nano-actuators

If nano-actuators are considered, eq. (10) would give a simple estimation of the resistance force to activate the system and slide a group of shells. This shows that our analysis could help in the future design of innovative low friction nanoscale linear actuators. Note that such an analysis can be extended considering a torque instead of the axial force, as may be useful for the design of rotational nano-actuators under rolling. The stress-analysis would remain basically the same, substituting the axial force with the torque, the Young's modulus with the shear elastic modulus, the displacement with the rotation and the cross-section area with the moment of inertia. In general, also different elastic moduli for the shells can be considered, substituting for linear actuators the cross section area with its product with the corresponding Young's modulus, or for rotational actuators the moment of inertia with its product with the corresponding shear modulus. For details, see /18/ and related references. For rotational actuators, in the energy balance no new surface area would be globally created, showing that a condition closer to the *superlubricating state* could arise in rotational rather than in linear nano-actuators. However, linear nano-actuators with a constant contact length during motion could also be designed. For such cases, eq. (5) would become $\Delta(W+T) = 0$ with ΔT proportional to the atomic heat dissipation.

Nanotube-based composites

Let us assume multi-walled nanotubes with $R_i \approx 0$ and define a critical pull-out stress for the external shell as $\sigma_{CPO} = \frac{F_{\max}}{2\pi R s}$, with F_{\max} given by eq. (10); for sufficiently long nanotubes we can assume asymptotic behaviour, i.e., $\vartheta \approx 1$. For example, for the first investigated nanotube, it corresponds to ~ 6 GPa. Then, we indicate the intrinsic strength of nanotubes as σ_{CN} (around ~ 100 GPa for ideal nanotubes; such a value must be divided by a factor of ~ 3.4 according to [20], if large holes (defects) are present). We define $\sigma_{CPO,CN}^* = \frac{2s}{R} \sigma_{CPO,CN}$, that is the mean value of the stress acting on the global cross section-area πR^2 , even if in reality only the external wall is under loading. Then, let us consider a matrix having strength σ_{CM} . Assume that in its cross-section are embedded an area fraction f_N of nanotubes that are going to break, a fraction area f_{PO} of nanotubes that are going to be pulled-out from their external shells, and a fraction area f_I of nanotubes that are going to break at the interface with the matrix (be pulled-out from the matrix). According to this last fracture mechanism, we can make a prediction of the corresponding required force, simply considering eq. (10) in which $R_e \rightarrow \infty$, and thus $\xi \rightarrow 1$, $\eta = 0$ (no sliding) and substituting $G_C^{(vdW)}$ with the fracture energy of the interface G_{CI} . Thus, for pulling-out a sufficiently long nanotube ($\vartheta \approx 1$) from a matrix, the force is predicted to be:

$$F_{\max}^{(asy)} = 2\pi R \sqrt{E R G_{CI}} \quad (12)$$

As previously stated, we can define $\sigma_{CI} = \frac{F_{\max}}{2\pi R s}$ and $\sigma_{CI}^* = \frac{2s}{R} \sigma_{CI}$. As a consequence, the prediction for the strength of the composite is:

$$\sigma_C \approx f_N \sigma_{CN}^* + f_{PO} \sigma_{CPO}^* + f_I \sigma_{CI}^* + (1 - f_N - f_{PO} - f_I) \sigma_{CM} \quad (13)$$

The fact that the force is basically length-independent means that pull-out of the nanotube cannot be avoided simply by increasing its length. Thus, a minimum radius is required to have a pull-out strength of the order of the intrinsic nanotube strength (from $\sigma_{CI} = \sigma_{CN}$):

$$R_{\min I} = \frac{\sigma_{CN}^2 s^2}{E G_{CI}} \quad (14a)$$

A similar consideration applies for the pull-out from the external shell (the minimum radius $R_{\min PO}$ can be deduced analogously from $\sigma_{CPO} = \sigma_{CN}$). To give an estimation for $R_{\min I}$, let us assume $\sigma_{CN} \approx 100$ GPa, $E \approx 1$ TPa, $G_{CI} \approx 1$ N/m ($s \approx 0.34$ nm), from which $R_{\min I} \approx 1$ nm. Thus, for practical

purpose, interface resistance can perhaps be comparable with the intrinsic strength of nanotubes.

In the same way, a prediction for the toughness of the composite can be obtained. Consider the fracture energy G_{CN} of the nanotube, estimated from the energy of the chemical bonds of the order of 10N/m, see /18/, and let us define $G_{CN}^* = \frac{2s}{R} G_{CN}$. The energy needed to pull-out a nanotube, from the external shell or from the matrix, is $\int_0^l F_{\max} dl \approx F_{\max}^{(asy)} l$; the sliding length l can be considered around one half the contact length. Accordingly, we define $G_{CPO,CI} = \int_0^l \sigma_{CPO,CI} dl \approx \sigma_{CPO,CI} l$ and $G_{CPO,CI}^* = \frac{2s}{R} G_{CPO,CI}$. For example, for the first carbon nanotube previously investigated, assuming $\vartheta \approx 1$ and $l \approx 7.5/2\mu\text{m}$, $G_{CPO} \approx 23\text{KNm}^{-1}$, that is three orders of magnitude larger than G_{CN} : thus, the pull-out of the nanotube represents a tremendously efficient mechanism to improve the toughness of the matrix (or its fracture energy G_{CM}). The fracture energy G_C of the composite can consequently be obtained as:

$$G_C = f_N G_{CN}^* + (f_{PO} + f_N) G_{CPO}^* + f_I G_{CI}^* + (1 - f_N - f_{PO} - f_I) G_{CM} \quad (15)$$

Note the presence of the term f_N that multiplies G_{CPO}^* . The reason is that the fractured nanotubes will also be pulled-out after fracture, from their external shells.

In addition, the Young's modulus of the composite E_C can be estimated from $E_C = fE^* + (1-f)E_M$, where $E^* = \frac{2s}{R}E$ (E is the Young's modulus of the nanotube), E_M is the Young's modulus of the matrix and $f = f_N + f_{PO} + f_I$.

Nanotube bundles

For bundles based on nanotubes the same concepts can be applied. We can consider this case as a limit case of a nanotube-based composite with negligible matrix and only van der Waals interactions. In this case, $G_{CI} \approx G_C^{(vdW)}$ (in eq. (12)) and $\sigma_{CM} \approx 0$, $G_{CM} \approx 0$ (in eqs. (13) and (15)) and $f = f_N + f_{PO} + f_I \neq 1$ is the fraction area corresponding to the bundle packaging, e.g., that we evaluate as ~ 0.9 if hexagonal. Note that assuming valid eq. (12) for bundles corresponds to assume moderate value for f_I (rigid "matrix").

If we consider a bundle (Fig. 8a) and we assume that $f_{PO} = 0$, the limit case (i) of $f_N = f$ would correspond to complete nanotube fracture (Fig. 8b), (ii) of $f_I = f$ to complete nanotube sliding (Fig. 8c), whereas in general (iii) the reality will be intermediate ($f_I + f_{PO} = f$, Fig. 8d). We note that such cases are the usually considered mechanisms for failure when evaluating the strength of a polymer crystal consisting of highly oriented polymer chains /25/.

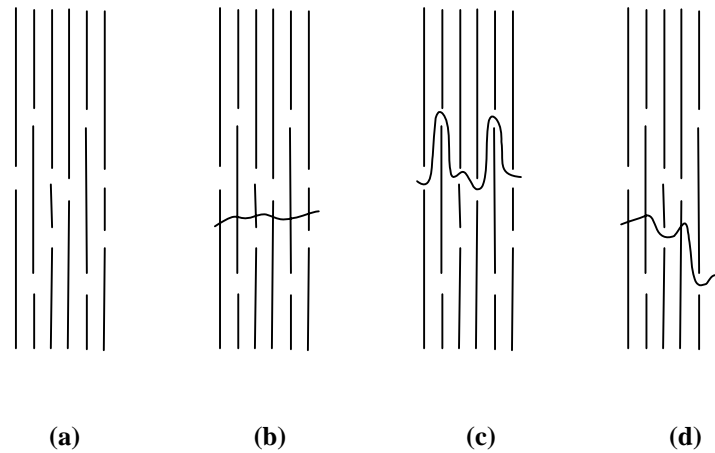


Fig. 8: (a).Nanotube-bundle (b).Nanotube fracture (c).Nanotube/interface pull-out (d). Intermediate case

From eq. (14), assuming $G_{CI} \approx G_C^{(vdW)}$ and the other values reported in the paper we estimate $R_{\min} \sim 5\text{nm}$, showing that defect-free bundles ($R \geq R_{\min}$, $l \geq l^{(asy)}$) could be very strong, even if including end effects—that is, finite sized nanotubes.

7. CONCLUDING REMARKS

We have shown that, in contrast to the common assumption, the contact force and shear stress are clearly not uniform along the contact length, as a consequence of boundary edge effects. Such effects dominate the sliding (stick-slip behaviour) at nanoscale, in a way more similar to a fracture phenomenon than to friction. We derive the relationship between contact-force and contact-length showing that it is asymptotic; this explains the difference in the experimental observations of nanotube sliding reported in literature. The analysis shows that different stick-slip motions can result in strongly different sliding forces (by one order of magnitude). Thus, the higher forces observed for sliding of the fractured outer shell nanotubes would correspond to larger sticking, probably due to the anchorage of the damaged external shell fracture “edge” rather than to the presence of an inner fracture end, as described in /16/. Finally, we have applied this analysis for predicting the strength and toughness of nanotube-based composites and nanotube-bundles. The pull-out phenomenon seems to provide a tremendously efficient mechanism for improving the toughness of the matrix, suggesting that nanotubes represent very promising nano-reinforcements. However, note that the simplified hypotheses assumed in the present analysis imply associated limitations in our findings.

ACKNOWLEDGEMENTS

The author thanks R. Ruoff and B. Curtin for discussion.

REFERENCES

1. Y.K. Kwon, D. Tomanek, S. Iijima, "Bucky Shuttle" memory device: Synthetic approach and molecular dynamics simulations, *Phys. Rev. Lett.*, **82**, 1470-1473 (1999).
2. M. Menon, D. J. Srivastava, Carbon nanotube based molecular electronic devices, *J. Mater. Res.*, **13**, 2357-2362 (1998).
3. G. Treboux, P. Lapstun, Z. Wu, K. Silverbrook, Interference-modulated conductance in a three-terminal nanotube system, *J. Phys. Chem. B*, **103**, 8671-8674, (1999).
4. R.E. Tuzun, D.W. Noid, B.G. Sumpter, R.C. Merkle, Dynamics of fluid flow inside carbon nanotubes, *Nanotechnology*, **7**, 241-246 (1996).
5. J. Han, A. Globus, R. Jaffe, G. Deardorff, Application of rigid-body dynamics and semiclassical mechanics to molecular bearings, *Nanotechnology*, **8**, 103-111 (1997).
6. R.E. Tuzun, K. Sohlberg, D.W. Noid, B.G. Sumpter, Docking envelopes for the assembly of molecular bearings, *Nanotechnology*, **9**, 37-48 (1998).
7. N. Pugno, Non-linear dynamics of nanotube based NEMS. *Recent research developments in sound and vibrations, Transworld Research Network*, **2**, 197-211 (2004).
8. S.Y. Akita, S. Nakayama, Y. Mizooka, T. Takano, Y. Okawa, S. Miyatake, S. Yamanaka, M. Tsuji, and T. Nosaka, Nanotweezers consisting of carbon nanotubes operating in an atomic force microscope, *Applied Physics Letters*, **79**, 1691-1693 (2001).
9. P. Kim, C. M. Lieber, Nanotube nanotweezers, *Science*, **126**, 2148-2150 (1999).
10. T. Rueckes, K. Kim, E. Joslevich, G. Y. Tseng, C. Cheung, C. M. Lieber, Carbon nanotube-based nonvolatile random access memory for molecular computing, *Science*, **289**, 94-97 (2000).
11. J. Kinaret, T. Nord, S. Viefers, A carbon-nanotube-based nanorelay, *Applied Physics Letters*, **82**, 1287-1289 (2003).
12. A. M. Fennimore, T. D. Yuzvlnsky, W. Q. Han, M. S. Fuhrer, J. Cummings, A. Zettl, Rotational actuator based on carbon nanotubes, *Nature*, **424**, 408-410 (2003).
13. A. Buldum, J.P. Lu, Atomic scale sliding and rolling of carbon nanotubes, *Phys. Rev. Lett.* **83**, 5050-5053 (1999).
14. M. R. Falvo, R. M. Taylor, A. Helser, V. Chi, F. P. Brooks Jr, S. Washburn and R. Superfine, Nanometre-scale rolling and sliding of carbon nanotubes, *Nature*, **397**, 236-238 (1999).
15. M.F. Yu, B.I. Yakobson, R.S. Ruoff, Controlled sliding and pullout of nested shells in individual

- multiwalled carbon nanotubes, *J. Phys. Chem. B*, **104**, 8764-8767 (2000).
16. S. Akita, Y. Nakayama, Extraction of inner shell from multiwall carbon nanotubes for scanning probe microscope tip, *Jpn. J. Appl. Phys.* **42**, 3933-3936 (2003).
 17. Z. Xia, W.A. Curtin, Pullout forces and friction in multiwall carbon nanotubes. *Phys. Rev. B*, **69**, 233408/1-4 (2004).
 18. N. Pugno, A. Carpinteri, Tubular adhesive joints under axial load, *J. of Appl. Mech.*, **70**, 832-839 (2003).
 19. A. Carpinteri, *Structural Mechanics: A Unified Approach*, E & FN Spon, 1997.
 20. N. Pugno, R. Ruoff, Quantized fracture mechanics. *Phil. Mag.*, **84**, 2829-2845 (2004).
 21. L. X. Benedict, N. G. Chopra, M. L. Cohen, A. Zettl, S. G. Louie, V. H. Crespi, Microscopic determination of the interlayer binding energy in graphite, *Chem. Phys. Letter*, **286**, 490-496 (1998).
 22. M. Hirano, K. Shinjo, Atomistic locking and friction, *Phys. Rev. B*, **41**, 11837-11851 (1990).
 23. M.F. Yu, O. Lourie, M.J. Dyer, K. Moloni, T.F. Kelly, R.S. Ruoff, Strength and breaking mechanism of multiwalled carbon nanotubes under tensile load, *Science*, **287**, 637-640 (2000).
 24. M.F. Yu, M.J. Dyer, R.S. Ruoff, Structure and mechanical flexibility of carbon nanotube ribbons: An atomic-force microscopy study, *J. of Appl. Phys.*, **89**, 4554-4557 (2001).
 25. B. Crist, The ultimate strength and stiffness of polymers, *Annu. Rev. Mater. Sci.*, **25**, 295-323 (1995).